

## Status and perspectives of cLFV at Mu2e

---

**Eleonora Diociaiuti on behalf of the Mu2e experiment<sup>a,\*</sup>**

<sup>a</sup>*Laboratori Nazionali di Frascati dell'INFN,  
Via Enrico Fermi 54, Frascati, Italy*

*E-mail: [eleonora.diociaiuti@lnf.infn.it](mailto:eleonora.diociaiuti@lnf.infn.it)*

Flavor physics offers a promising way to explore fundamental aspects of the standard model, such as the mass hierarchy and electroweak symmetry breaking. Within this field, Charged Lepton Flavor Violation (CLFV) stands out as a phenomenon that is strongly suppressed in the Standard Model, making it an excellent probe for potential new physics. Ongoing CLFV experiments, including Mu2e, COMET, MEG, and Mu3e, are preparing for data collection in the coming decade. Among the possible searches in the muon sector ( $\mu \rightarrow e\gamma$ ,  $\mu 3e$  and muon conversion), two muon conversion experiments will start taking data in few years: Mu2e at Fermilab and COMET at JPark. Both of them aim to improve the current sensitivity by several orders of magnitude. This violation of charged lepton flavor presents an opportunity to explore novel physics on a scale not currently accessible through direct searches at contemporary or planned high-energy colliders.

*Workshop Italiano sulla Fisica ad Alta Intensità (WIFAI2023)  
8-10 November 2023*

*Dipartimento di Architettura dell'Università Roma Tre, Rome, Italy*

---

\*Speaker

## 1. Introduction

In the pursuit of uncovering Physics beyond the Standard Model (SM), an effective path is exploring new interactions that manifest in rare processes prohibited by the SM, commonly categorized as the “intensity frontier”. The Mu2e experiment aligns with a global initiative to investigate Charged Lepton Flavor Violating (CLFV) processes. The observation of such processes would serve as compelling evidence for the existence of new Physics beyond the SM. Within the muon sector, the  $\mu N \rightarrow e N$  process is often regarded as the “golden channel” due to its distinct signature and substantial discovery potential. The signature of the  $\mu N \rightarrow e N$  process yields a monochromatic  $e^-$  with an energy just below the rest mass of  $\mu$ , specifically  $E_e = m_\mu c^2 - B.E. - E_{recoil} = 104.97 \text{ MeV}$ , considering the combined effects of the  $\mu$ -binding energy and the recoil of the nucleus [1].

The current best limit on the conversion process, evaluated as:

$$R_{\mu e} = \frac{\Gamma(\mu^- + N(A, Z) \rightarrow e^- + N(A, Z))}{\Gamma(\mu^- + N(A, Z) \rightarrow \nu_\mu + N(A, Z - 1))} < 7 \times 10^{-13} \text{ (90\% CL)}$$

has been set by the Sindrum-II collaboration. Mu2e aims to improve it by four orders of magnitude [2].

## 2. The experimental setup

As shown in Figure 1 the Mu2e experiment is composed of a system of three superconducting solenoids [3].

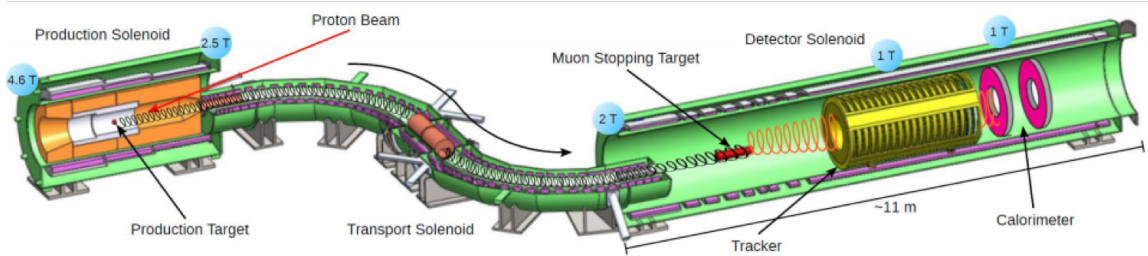


**Figure 1:** Schematic view of the Mu2e apparatus

An 8 GeV pulsed proton beam, extracted from the Fermilab Delivery Ring, interacts with the  $\sim 1.6\lambda$  long tungsten production target, positioned in the center of the first superconducting solenoid: the Production Solenoid (PS). The PS generates a graded magnetic field ranging from 4.5T to 2.5T, enhancing the acceptance of adjacent magnetic components, notably the Transport Solenoid (TS), particularly for low-momentum particles. The TS, designed with a distinctive “S” shape, employs a graded toroidal field (ranging from 2.5T to 2T) and a set of rotatable collimators to selectively filter charged particles based on their desired momentum. Two absorber windows positioned at the TS entrance and midpoint effectively suppress antiproton background. The final solenoid, the Detector Solenoid (DS), accommodates the aluminum stopping target and is surrounded by two proton absorbers that mitigate radiation within the detector region housing the Straw Tube tracker

and electromagnetic calorimeter. The DS also features a graded magnetic field transitioning from 2T to 1T. The magnetic field in the tracker-calorimeter region is uniform at 1T, ensuring optimal accuracy in momentum reconstruction. The beam pulsed structure is depicted in Figure 2.

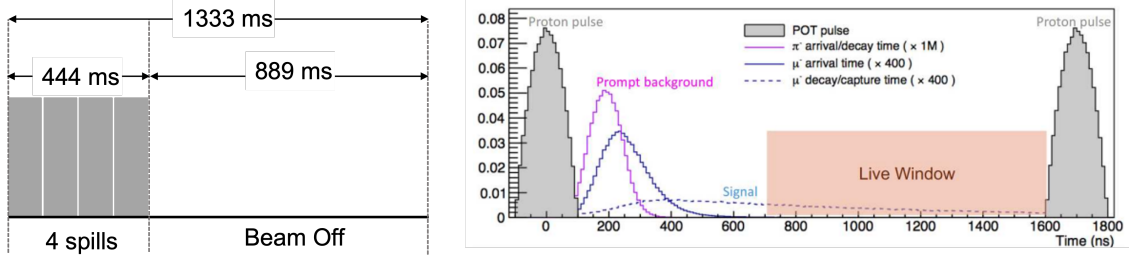


**Figure 2:** Left: 1.4 s structure of the main injector cycle and proton beam fraction delivered to Mu2e. Right: Mu2e pulsed proton beam structure.

As shown in Figure 2 (Left), the duration of the main injector cycle is  $\sim 1.4$  s, the Mu2e primary protons are continuously delivered for about 0.4 s, after that the proton beam is off in the experimental all the remainder of the cycle. The proton beam features a pulsed structure with 250 ns-wide proton pulses separated by 1695 ns. The lifetime of an Al atom ( $\tau = 864$  ns) allows to open a retarded acquisition window  $\sim 700$  ns after the proton spill, facilitating the collection of a good fraction of the possible Conversion Electrons (CE) while effectively eliminating the prompt backgrounds. The fraction of protons out of spill should be kept at a level lower than  $10^{-10}$ , it will be monitored by a detector observing the particles scattered from the production target.

The Stopping Target (depicted in Figure 3 Left) comprises 37 aluminum disks, each 100  $\mu\text{m}$  thick. The segmented structure serves to minimize the material traversed by the CE before it reaches the tracker. The straw tube tracker [4] (shown in Figure 3 Right) adopts an annular configuration with

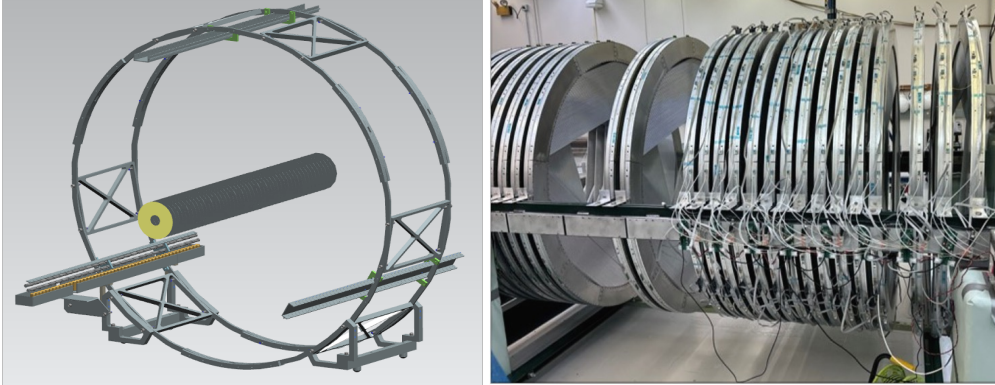


**Figure 3:** Left: sketch of the Stopping Target. Right: View of the tracker construction status.

an outer radius of 70 cm, an inner radius of 38 cm, and a total length of approximately 3.3 m. It consists of 18 stations, each composed of 2 planes with 3 panels each. Each panel, consisting of a double layer of straw tubes with varying lengths, covers a  $120^{\text{deg}}$  circular segment. The tubes have a diameter of 5 mm, a thin mylar wall measuring 15  $\mu\text{m}$ , and a tungsten anode wire of 25  $\mu\text{m}$  at 1450 V. They are filled with an 80%-20% Ar-CO<sub>2</sub> gas mixture, and are read by ADCs and TDCs at both ends.

The electromagnetic calorimeter [5] (see Figure 4 Left) is composed of two annular disks, each filled of 674 pure CsI crystals with dimensions of  $34 \times 34 \times 200 \text{ mm}^3$ . The primary purpose of the calorimeter is to discriminate against cosmic ray muons that mimic the conversion electron signal: from simulation, it is expected that there will be an CE-like event produced every day, i.e. a cosmic muon converting in the Al Stopping Target at producing an electron with energy within the signal region. A particle identification ANN classifier utilizes the particle time of flight from the tracker to the calorimeter and the ratio between the calorimeter-measured energy and the tracker-measured momentum. This classifier effectively suppresses muons by a factor exceeding 100, while introducing negligible inefficiency for the electron signal. The disks, featuring an inner radius of 374 mm and an outer radius of 660 mm, are separated by 700 mm, allowing the second disk to capture electrons passing through the hole in the first one. Each crystal is coupled with two arrays of 6 SiPMs for readout. Preamplifier boards are positioned directly behind the SiPMs, while the slow control and digital electronics are housed in crates surrounding the disks. Despite approximately one cosmic ray event per day mimicking a 105 MeV/c electron, a significant portion of this background is eliminated by the Cosmic Ray Veto (CRV) system [6], shown in (see Figure 4 Right). This system comprises four layers of scintillator counters, read by wavelength shifter fibers, surrounding the DS and the last segment of the TS. Each fiber is read at both ends by SiPMs. The CRV is expected to identify 99.99% of charged cosmic particles traversing it. This demanding performance will be monitored through an extensive dataset acquired with the beam off during regular operations.

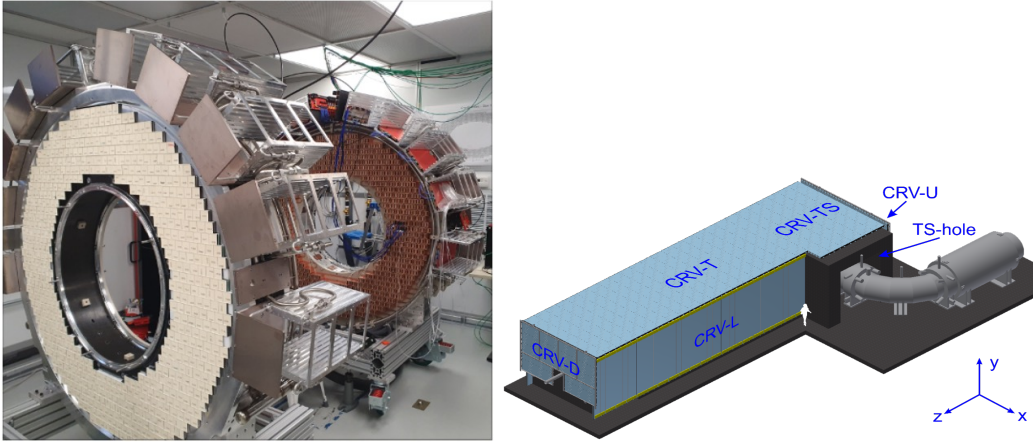


**Figure 4:** Left: Status of the construction of the calorimeter disks. Right: Sketch of the Cosmic Ray Veto.

### 3. $Mu2e$ Sensitivity

$Mu2e$  is scheduled to operate in two distinct phases [7]: Run 1 is set to occur from the last quarter of 2026 up to the first quarter of 2027, while Run 2 is foreseen to span approximately 3 years following the accelerator shutdown for the construction of the Long-Baseline Neutrino Facility facility. Notably, Run 2 will feature a doubled beam duty cycle compared to Run 1. The sensitivity of the Run 1 experiment has recently been refined to  $SES = 2.4 \times 10^{-16}$ , incorporating the outcomes of tests on the initial subdetector prototypes. Additionally, enhancements have been

made to the analysis software, focusing on track quality selection, particle identification, and cosmic rejection. The “ $5\sigma$  discovery sensitivity” of the experiment has undergone optimization through the exploration of potential momentum and time selection windows, as illustrated in Figure 5.

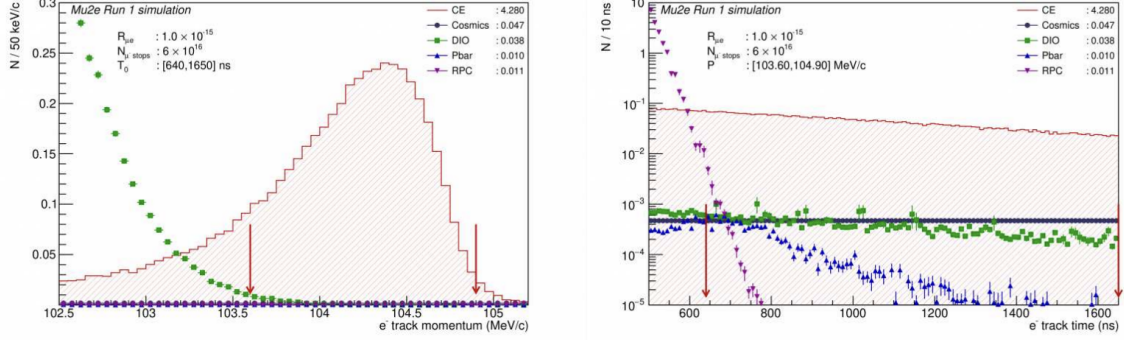


**Figure 5:** Run 1 expected momentum (left) and time (right) distributions for the CE signal (assuming  $R_{\mu e} = 10^{-15}$ ) and the main backgrounds. The red arrows indicate the optimized analysis cuts.

A list of the principal background for Run1 can be found in Table 1.

Channel	Mu2e Run 1
Cosmic rays	$0.046 \pm 0.010$ (stat) $\pm 0.009$ (syst)
DIO	$0.038 \pm 0.002$ (stat) $^{+0.025}_{-0.015}$ (syst)
Antiprotons	$0.010 \pm 0.003$ (stat) $\pm 0.010$ (syst)
RPC in time	$0.010 \pm 0.002$ (stat) $^{+0.001}_{-0.003}$ (syst)
RPC out-of-time ( $\zeta = 10^{-10}$ )	$(1.2 \pm 0.1$ (stat) $^{+0.1}_{-0.3}$ (syst)) $\times 10^{-3}$
RMC	$< 2.4 \times 10^{-3}$
Decays in flight	$< 2.0 \times 10^{-3}$
Beam electrons	$< 1 \times 10^{-3}$
Total	$0.105 \pm 0.032$

**Table 1:** Background summary using the optimized signal momentum and time window,  $103.60 < p < 104.90$  MeV/c and  $640 < T_0 < 1650$  ns.

The primary source of background arises from cosmic rays, predominantly muons entering through the TS hole and interacting within the TS material, leading to the production of electrons. The time distribution of these electrons is uniform. The second significant background is attributed to muon Decays In Orbit (DIO) occurring in the stopping target. As shown in Figure 5 the Michel spectrum of electrons from  $\mu$  decay gets significantly modified by interaction with the nucleus, resulting in the presence of a recoil tail with a fast falling slope close to the  $\mu$ -e conversion endpoint. Other important background to mitigate are the antiprotons and the Radiative Pion Captures: antiprotons can annihilate in the stopping target or produce pions in the TS. This background can only be reduced with the use of absorbers placed along the beam line. For what concerns RPC, non-decayed pions can reach the stopping target and then can be radiatively captured. The photons emitted during this process can undergo internal or external conversion, resulting in electrons. The

time distribution of these electrons is characterized by an early peak, which can be effectively mitigated by implementing a time cut.

#### 4. Comet Status

The Comet experiment [8] schedule is divided into three different phases. The layout of each phase of the experiment is reported in Figure 6

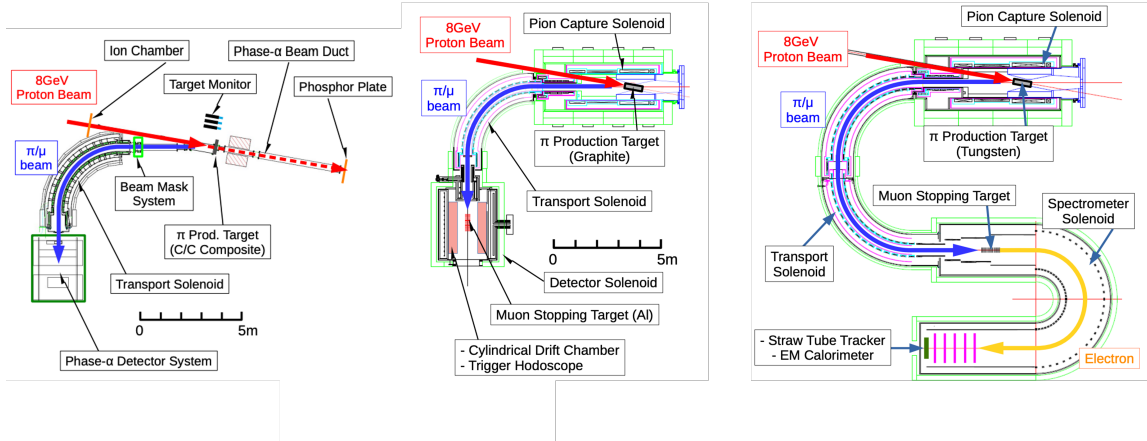


**Figure 6:** Three phases of the COMET experiment: Phase  $\alpha$  (left), Phase-I (center), and the proposed Phase-II (right).

The J-PARC accelerator will deliver an 8 GeV proton beam directed into the Pion Production Target, a 700 mm-long graphite assembly housed within the Pion Capture Solenoid. Pions produced in this target undergo decay into muons during their transport through the Transport Solenoid. Subsequently, muons are brought to a halt at the aluminum stopping target, and the momentum of the resulting decay electrons is precisely measured using the Cylindrical Drift Chamber (CDC). Expected sensitivity for this phase is set at  $7 \times 10^{-15}$ , representing a remarkable 100-fold enhancement. An additional focus during Phase-I involves the investigation of the secondary beam itself, aiming to set background levels for the subsequent Phase-II. To facilitate this study, the Muon stopping target and CDC are replaced with the Straw Tube Tracker and EM Calorimeter. It's noteworthy that the identical detector setup planned for Phase-II will be employed in this secondary beam analysis. Phase  $\alpha$  have been carried out between February and March 2023 to test transport of the secondary beam: proton beam was successfully extracted into the COMET beam hall and the first observation of muon beam successfully transported via a  $90^\circ$ -curved Muon Transport Solenoid was achieved.

#### 5. Conclusion

Mu2e and COMET are discovery experiments looking for the cLFV process of a coherent conversion of muon into electron. The Mu2e goal is to improve the current sensitivity of  $\sim 4$  orders of magnitude, providing discovery capabilities over a wide range of NP models, and allowing to explore mass scales up to 10000 TeV. The installation of the detectors is foreseen in 2024; commissioning will follow in 2025.

## Acknowledgements

We are grateful for the vital contributions of the Fermilab staff and the technical staff of the participating institutions. This work was supported by the US Department of Energy; the Istituto Nazionale di Fisica Nucleare, Italy; the Science and Technology Facilities Council, UK; the Ministry of Education and Science, Russian Federation; the National Science Foundation, USA; the National Science Foundation, China; the Helmholtz Association, Germany; and the EU Horizon 2020 Research and Innovation Program under the Marie Skłodowska-Curie Grant Agreement Nos. 734303, 822185, 858199, 101003460, and 101006726. This document was prepared by members of the  $Mu2e$  Collaboration using the resources of the Fermi National Accelerator Laboratory (Fermilab), a U.S. Department of Energy, Office of Science, HEP User Facility. Fermilab is managed by Fermi Research Alliance, LLC (FRA), acting under Contract No. DE-AC02-07CH11359.

## References

- [1] Bernstein, Robert H. et al, Charged Lepton Flavor Violation: An Experimenter's Guide, Phys. Rep.,532, 2, 27-64, 2013
- [2] Bertl, W. et al, A search for  $\mu$ -  $e$  conversion in muonic gold, EPJ C, 47, 337A ,S346, 2006
- [3] L. Bartoszek et al., "The  $Mu2e$  Collaboration,  $Mu2e$  technical design report," ArXiv:1501.05241, 2015.
- [4] M. J. Lee for the  $Mu2e$  collaboration, "The straw tube tracker for the  $Mu2e$  experiment," Nucl. Phys. B. Proc. Suppl., vol. 273-275, 325
- [5] N. Atanov et al., "Design and status of the  $Mu2e$  calorimeter," IEEE-TNS 65, pp. 2073-2080, 2018, ArXiv:1802.06346.
- [6] A. Artikov et al. ( $Mu2e$  CRV group), ArXiv:1511.00374 (2015).
- [7]  $Mu2e$  Collaboration.  $Mu2e$  run I sensitivity projections for the neutrinoless  $\mu^- \rightarrow e^-$  conversion search in aluminum. Universe 9.1 (2023): 54.
- [8] Jansen A . "Status of the COMET experiment" EPJ Web of Conferences. Vol. 282. EDP Sciences, 2023.